National Défense
Defence nationale

UNCLASSIFIED
UNLIMITED DISTRIBUTION

DREV REPORT 4389/86
FILE: 3621J-010
FEBRUARY 1986

CRDV RAPPORT 4389/86
DOSSIER: 3621J-010
FÉVRIER 1986

REAL-TIME SIMULATION OF CRUCIFORM SHORT-RANGE AIR-TO-AIR GUIDED MISSILES

A. Morin

RESEARCH AND DEVELOPMENT BRANCH
DEPARTMENT OF NATIONAL DEFENCE
CANADA

BUREAU - RECHERCHE ET DÉVELOPPEMENT
MINISTÈRE DE LA DÉFENSE NATIONALE
CANADA

Defence Research Establishment
Centre de recherches pour la Défense,
• Valcartier, Québec

SANS CLASSIFICATION
DISTRIBUTION ILLIMITÉE

Canada

DREV R-4389/86
FILE: 3621J-010

UNCLASSIFIED

CRDV R-4389/86
DOSSIER: 3621J-010

REAL-TIME SIMULATION OF CRUCIFORM SHORT-RANGE AIR-TO-AIR GUIDED MISSILES

by

A. Morin

DEFENCE RESEARCH ESTABLISHMENT

CENTRE DE RECHERCHES POUR LA DÉFENSE

VALCARTIER

Tel: (418) 844-4271

Québec, Canada

February/février 1986

SANS CLASSIFICATION

ABSTRACT

A six-degree-of-freedom missile simulation has been carried out in real time by a digital multiprocessor. The missile model and the simulation are described in this report. The simulation has also been verified by open- and closed-loop tests.

RÉSUMÉ

La simulation d'un missile comportant six degrés de liberté a été réalisée en temps réel à l'aide d'un multiprocesseur numérique. Le modèle du missile et la simulation sont décrits dans ce rapport. La simulation a aussi été vérifiée par des essais en boucle ouverte et fermée.

TABLE OF CONTENTS

ABSTRACT/RÉSUMÉ 1

LIST OF VARIABLES v

1.0 INTRODUCTION 1

2.0 MODEL OF THE MISSILE SIMULATION 1

2.1 Model of the Seeker 2
2.2 Model of the Airframe 5
2.3 Missile Control 7
2.4 Model of the Missile-Target Geometry 11
2.5 Miss Distance 13

3.0 SIMULATION OVERVIEW 13

4.0 SIMULATION RESULTS 17

5.0 CONCLUSION 23

6.0 REFERENCES 25

TABLE I

FIGURES 1 to 13

APPENDIX A - Coordinate Systems and Coordinate Systems Rotations 26
APPENDIX B - Missile Aerodynamics 38
APPENDIX C - Missile-Target Geometry 44
APPENDIX D - Description and Operation of Digital Multiprocessor AD-10 47

I_X, I_Y, I_Z	Missile moments of inertia about roll, pitch and yaw axes
K_1	Forward (open loop) gain of the tracking system
K_2	Tracking-system responsivity
K_3	Gain of the missile damping system
K_A, K_B, K_C	Gain of the control-surface servopositioner system
K_L	Steering-system responsivity
K_R	Gain of the missile roll control
m	Mass of missile
M_X, M_Y, M_Z	External moments in the (X_B, Y_B, Z_B) coordinate system acting on the missile
MD	Miss distance
q	Dynamic pressure
R	Missile-target range
S	Cross-sectional area of missile body
s	Laplace operator
T	Thrust force
u, v, w	Components of missile velocity along the (X_B, Y_B, Z_B) axes
V_C	Missile-target closing velocity
V_M	Missile velocity
V_{SP}, V_{SY}	Output signal of the tracking system (seeker) in the pitch and yaw channels
V_{AP}, V_{AY}	Output signal of the guidance filter
V_i	Input signal of the control-surface servopositioner
V_s	Speed of sound
V_T	Target velocity

LIST OF VARIABLES

C_{D0}	Missile coefficient of drag
$C_{D\alpha^2}$	Missile drag stability derivative due to angles of attack
$C_{D\delta^2}$	Missile drag stability derivative due to control-surface deflection angles
$C_{D\alpha\delta}$	Missile drag stability derivative due to angle of attack and control-surface deflection angles
$C_{\ell\alpha\alpha}$	Missile rolling moment stability derivative due to the angles of attack in the missile pitch and yaw planes
$C_{\ell\alpha\delta}$	Missile rolling moment stability derivative due to an angle of attack in one missile plane and a control-surface deflection in the opposite missile plane
$C_{\ell\delta}$	Missile rolling moment stability derivative due to control-surface deflection angle
$C_{\ell\dot{\theta}}$	Missile rolling moment stability derivative due to missile roll rate
$C_{L\alpha}$, $C_{L\delta}$	Missile lift stability derivatives due to angle of attack and control-surface deflection angle
$C_{m\alpha}$, $C_{m\delta}$	Missile pitching moment stability derivatives due to angle of attack and control-surface deflection angle
$C_{m\dot{\theta}}$, $C_{m\dot{\alpha}}$	Missile pitching moment stability derivatives due to missile pitching rate and angle of attack rate
d	Diameter of the missile body
$f_1(\alpha_p, \alpha_y)$	Variable which varies as functions of the angles of attack
$f_2(\alpha, \delta)$	Variable which varies as functions of the angle of attack and of the control-surface deflection angle
F_X, F_Y, F_Z	External forces in the (X_B, Y_B, Z_B) coordinate system acting on the missile
g	Acceleration of gravity
H	Missile angular momentum

V_X, V_Y, V_Z	Components of the missile-target closing velocity along the (X, Y, Z) axes
X, Y, Z	Earth-fixed coordinate system
X_B, Y_B, Z_B	Body-coordinate system
X_L, Y_L, Z_L	Line-of-sight coordinate system
X_S, Y_S, Z_S	Seeker-coordinate system
X_V, Y_V, Z_V	Missile-velocity coordinate system
X_M, Y_M, Z_M	Missile position in the earth-fixed coordinate system
X_T, Y_T, Z_T	Target position in the earth-fixed coordinate system
α_P, α_Y	Missile angles of attack in the body-coordinate system
β	Angle between the range vector and the missile-target closing velocity in the earth-fixed coordinate system
γ_A, γ_E, γ_R	Euler angles used to represent the missile velocity vector in the earth-fixed coordinate system
γ_p, γ_Y, γ_r	Angles of the missile velocity vector in the missile-velocity coordinate system
δ_p, δ_Y, δ_R	Angles of control surfaces which modify the pitch, yaw and roll motions of the missile
δ_{pA}, δ_{pB}	Angles of the two independent control-surface servos of the pitch channel
ϵ_p, ϵ_Y	Error angles between the line of sight and the seeker
θ_A, θ_E, θ_R	Euler angles to represent the missile body in the earth-fixed coordinate system
θ_p, θ_Y, θ_r	Euler angles to represent the missile body in the body-coordinate system
λ_p, λ_Y	Error angles between the seeker and the body of the missile
ρ	Atmospheric density
σ_A, σ_E	Angles that represent the line of sight in the earth-fixed coordinate axes

σ_p, σ_Y	Angles that represent the line of sight in the line-of-sight coordinate axes' system
τ_1	Time constant of the seeker receiver (signal processor)
τ_2	Time constant of the torque servo of the seeker
τ_3	Time constant of the magnetic driver of the control-surface servopositioner
τ_4, τ_5	Time constants of the roll control system
τ_6, τ_7, τ_8, τ_9	Time constants of the control for damping the body of the missile
τ_L	Steering-filter time constant
ϕ_A, ϕ_E, ϕ_R	Euler angles that represent the seeker in the earth-fixed coordinate system
ϕ_p, ϕ_Y, ϕ_r	Angles of the seeker in the seeker-coordinate system

1.0 INTRODUCTION

This document describes a six-degree-of-freedom (6 DOF) missile simulation which was developed at Defence Research Establishment Valcartier (DREV). The missile implemented in this simulation is a small supersonic air-to-air missile which is guided to the target by means of a proportional navigation law. Maneuvering control is achieved by four surfaces in cruciform configuration located at the rear of the missile and hinged on fixed stabilizing fins. The simulation includes a simplified model of the seeker, a linearized aerodynamic model which assumes small angles of attack, a linearized model of the control system, missile-target kinematics and a miss-distance computation. The simulation does not consider noise in the seeker and control system and all the missile instruments are assumed to be ideal components. The simulation is performed in real time on the AD-10 digital multiprocessor manufactured by Applied Dynamic International.

This document presents the development of the missile model to be simulated and reports the tests which were performed on the simulation. In a first set of tests, open-loop simulations were performed to check the operation of the aerodynamics and the control system of the missile. In a second procedure, the operation of the missile guidance was verified by simulating in a closed loop typical missile-target engagements. The target and missile trajectories were then output and analyzed. This work was performed at DREV between April 1983 and December 1984 under PCN 21J10, Simulation of Missile Guidance and Control Systems.

2.0 MODEL OF THE MISSILE SIMULATION

The missile simulation consists of a simplified model for the seeker, a linearized second-order actuator for the control of the fins' aerodynamic surface, a roll control and a control for damping the body of the missile by means of three rate gyroscopes. The simulation also

includes a nonlinear model of the airframe and differential equations describing the missile-target kinematics. The target intercept problem is solved through a proportional navigation guidance law. It is a type of guidance in which the rate of rotation of the missile velocity vector is made linearly proportional to the observed rate of rotation of the line of sight (LOS) to the target so as to reduce the LOS rotation.

The simulation model of the air-to-air missile for the pitch plane is shown in Fig. 1. The error between the LOS and the seeker is sensed by the seeker detector. This error is processed and the gyro gimbals are torqued to reduce it. The seeker output, which is proportional to the LOS rate, feeds the guidance filter. Its gain is made variable with the launching altitude in order to maintain the navigation constant at a fixed value. The resulting signal goes through the control and aerodynamics where the missile velocity V_M and its angle γ are derived. After the body axis-to-inertial axis transformation, the data V_M and γ are combined to the target simulator to yield the range and the LOS angle. Finally, the loop is closed by the inertial axis-to-seeker axis transformation of the LOS angle.

2.1 Model of the Seeker

Whatever the missile-to-target interaction is, the purpose of the seeker is to receive energy from the target and to produce signals which are proportional to the error between the LOS and the position of the seeker. An extremely simplified tracking loop model (Ref. 1) is utilized in the simulation. The seeker hardware consists essentially of a two-degree-of-freedom gyroscope with an optical system and a detector mounted directly upon it. The energy from the target is detected and processed by the seeker. The gyro gimbals are torqued to reduce the error between the LOS and the position of the seeker.

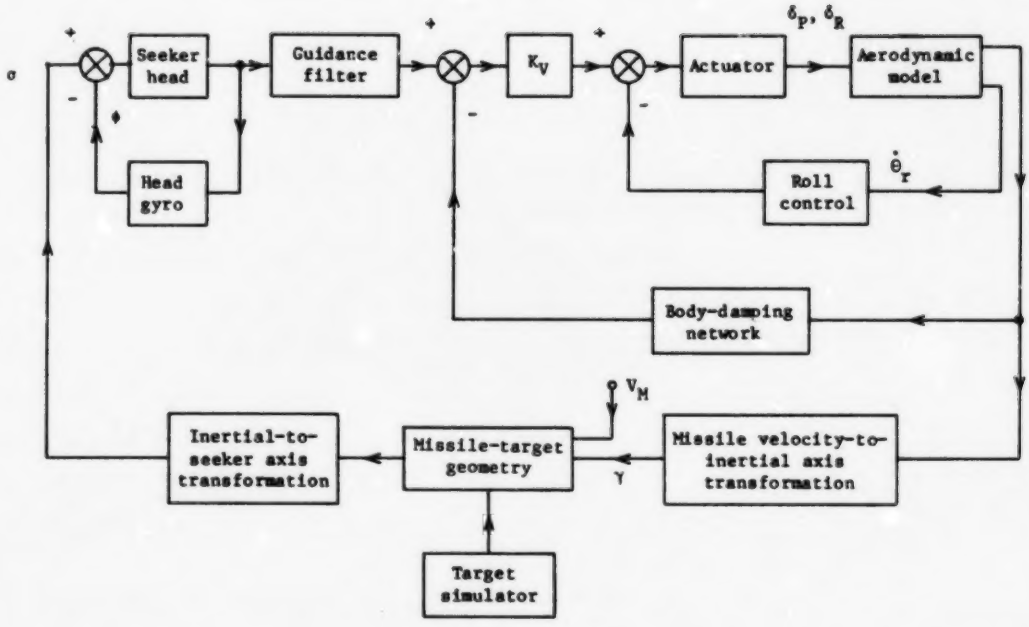

FIGURE 1 - Block diagram of the missile simulation. In this schematic only the pitch channel is illustrated. The yaw channel is identical, except that the loop of the roll control is not included.

A block diagram of the tracking loop servo for the pitch channel, which is identical to the yaw channel, is shown in Fig. 2. The detector and its associated circuitry develop a steering signal V_S proportional to the angle ε between the gyro axis and the target LOS, that is:

$$V_{SP} = \frac{K_1 \varepsilon_P}{\tau_1 s + 1} \text{ and } V_{SY} = \frac{K_1 \varepsilon_Y}{\tau_1 s + 1} \qquad [1]$$

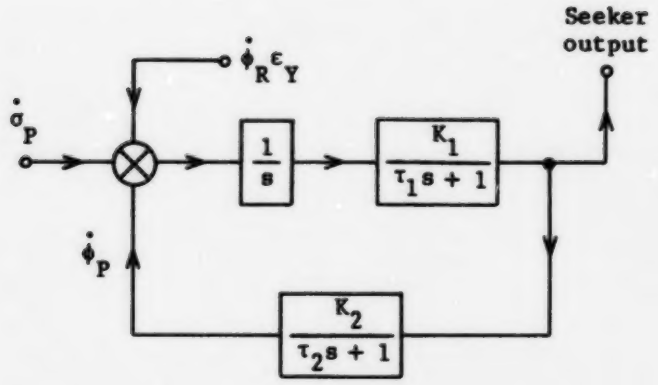

FIGURE 2 - Simplified model of the seeker

Applying torque to the gyro causes precession with respect to free space at a rate proportional to V_S and then tends to reduce ε:

$$\dot{\phi}_P = \frac{K_2 \, V_{SP}}{\tau_2 s + 1} \text{ and } \dot{\phi}_Y = \frac{K_2 \, V_{SY}}{\tau_2 s + 1} \qquad [2]$$

Thus, the LOS is tracked and a measure of the spatial rate of rotation of the target is obtained. In the simulation it is assumed that the field of view of the seeker is limited to 3°. The output of the seeker will be linear for error angles varying from -3° to 3°.

The rate of the error angles $\dot{\varepsilon}_p$ and $\dot{\varepsilon}_y$ are derived in Appendix A by the seeker-to-line-of-sight coordinate transformation. It is given by:

$$\dot{\varepsilon}_p = \dot{\sigma}_p - \dot{\phi}_p - \dot{\phi}_r \, \varepsilon_y \qquad [3]$$

$$\dot{\varepsilon}_y = \dot{\sigma}_y - \dot{\phi}_y + \dot{\phi}_r \varepsilon_p \qquad [4]$$

where $\dot{\phi}_r$ is a relation obtained in Appendix A after a seeker-to-body coordinate rotation:

$$\dot{\phi}_r = \sin \lambda_P(\dot{\lambda}_P(\dot{\lambda}_Y + \dot{\theta}_Y)) + \dot{\theta}_r \cos \lambda_Y \cos \lambda_P + \dot{\theta}_P \sin \lambda_Y \cos \lambda_P \quad [5]$$

2.2 Model of the Airframe

The airframe model, completely described in Appendix B, includes translational and rotational dynamics and generation of aerodynamic forces and moments. Airframe dynamics are simulated in 6 DOF with the missile orientation represented by three Euler angles. Maneuvering control was achieved by means of four surfaces in cruciform configuration located at the rear of the missile and hinged on fixed stabilizing fins.

In deriving the equations of motion of the airframe, the following assumptions were made:

1) Body axes are the principal axes of inertia.

2) Mass distribution is the same about the Y_B and Z_B axes, producing equal moments of inertia about these axes.

3) Rotational and translational motions are referenced to the center of gravity.

4) Small angle approximation was used for the aerodynamic angles of attack, α_P and α_Y, since we assume that these angles do not exceed 20°.

5) Second-order aerodynamic coefficient derivatives ($C_{D\delta^2}$, $C_{D\alpha\delta}$, $C_{m\alpha\delta}$, $C_{m\alpha^2}$) and the dynamic coefficient derivative $C_{m\dot{\alpha}}$ were not considered in the simulation.

Under these assumptions, the following equations hold:

$$\dot{V}_M = (F_X - F_Y\alpha_Y - F_Z\alpha_P)/m \qquad [6]$$

$$\dot{\gamma}_P = \frac{qS}{mV_M}(C_{L\alpha}\alpha_P + C_{L\delta}\delta_P + \frac{F_X\alpha_P}{mV_M} - \frac{g}{V_M}\cos\theta_E\cos\theta_R) \qquad [7]$$

$$\dot{\gamma}_Y = \frac{qS}{mV_M}(C_{L\alpha}\alpha_Y + C_{L\delta}\delta_Y + \frac{F_X\alpha_Y}{mV_M} - \frac{g}{V_M}\cos\theta_E\sin\theta_R) \qquad [8]$$

$$\ddot{\theta}_P = -\frac{qSd}{I_Y}[C_{m\alpha}\alpha_P + C_{m\delta}\delta_P + \frac{d}{V_M}(C_{m\dot{\theta}}\dot{\theta}_P)] - \frac{(I_X - I_Z)}{I_Y}\dot{\theta}_Y\dot{\theta}_r \qquad [9]$$

$$\ddot{\theta}_Y = -\frac{qSd}{I_Z}[C_{m\alpha}\alpha_Y + C_{m\delta}\delta_Y + \frac{d}{V_M}(C_{m\dot{\theta}}\dot{\theta}_P)] - \frac{(I_Y - I_X)}{I_Z}\dot{\theta}_P\dot{\theta}_r \qquad [10]$$

$$\ddot{\theta}_R = -\frac{qSd}{I_X}[C_{\ell\delta}\delta_R + f_1(\alpha_P,\alpha_Y)C_{\ell\alpha\alpha} + f_2(\alpha,\delta)C_{\ell\alpha\delta} + \frac{d}{V_M}C_{\ell\dot{\theta}}\dot{\theta}_R] \qquad [11]$$

Forces F_X, F_Y and F_Z are derived in Appendix B.

The angles $\dot{\alpha}_P$ and $\dot{\alpha}_Y$ are derived from the body-to-missile velocity coordinate rotation (Appendix A):

$$\dot{\alpha}_p = \dot{\theta}_p - \dot{\gamma}_P + \dot{\theta}_r\alpha_Y \qquad [12]$$

$$\dot{\alpha}_Y = \dot{\theta}_Y - \dot{\theta}_Y - \dot{\theta}_r\alpha_p \qquad [13]$$

The body-to-inertial coordinate rotation (Appendix A) is also used in the computation of eqs. 6 to 10. This yields:

$$\dot{\theta}_E = \dot{\theta}_p\cos\theta_R + \dot{\theta}_Y\sin\theta_R \qquad [14]$$

$$\dot{\theta}_A = (\dot{\theta}_Y \cos \theta_R - \dot{\theta}_p \sin \theta_R)/\cos \theta_E \qquad [15]$$

$$\dot{\theta}_R = \dot{\theta}_r - \dot{\theta}_A \sin \theta_E \qquad [16]$$

2.3 Missile Control

The control system of the pitch and yaw channels, shown in Figs. 3 and 4 respectively, provides the following basic functions:

a) deflection of control surfaces in proportion to the steering voltages generated by the tracking system;

b) limitation of control-surface deflection;

c) roll rate control; and

d) control for damping the aerodynamic response.

In the present simulation, we assume that the rate gyros are ideal components so that their measure corresponds to the missile body rates $\dot{\theta}_p$, $\dot{\theta}_Y$ and $\dot{\theta}_r$ given by the aerodynamic responses.

2.3.1 Guidance Filter

The guidance filter is a first-order system with the following transfer function:

$$\frac{V_{AP}}{V_{SP}} \left(\text{and } \frac{V_{AY}}{V_{SY}}\right) = \frac{K_L}{\tau_L s + 1} \qquad [17]$$

where K_L is the gain which adjusts, as a function of the launching altitude, the steering channel gain so that the navigation parameter remains constant.

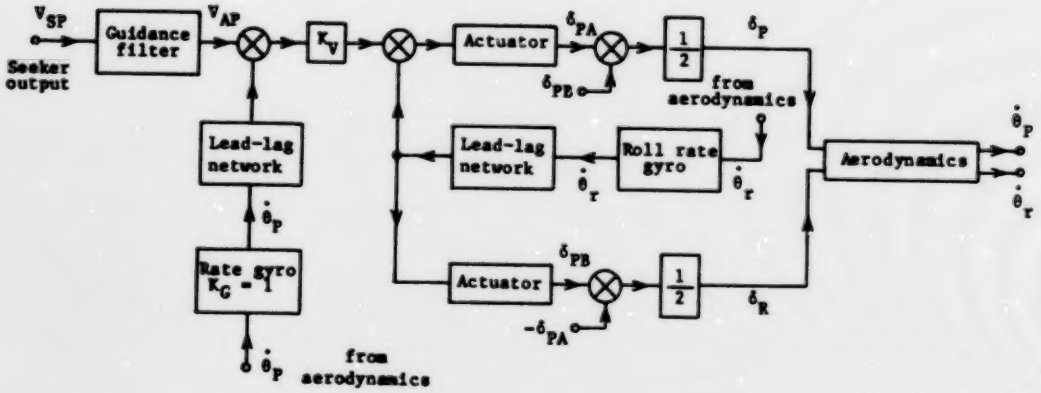

FIGURE 3 - Control of the pitch channel (with roll control)

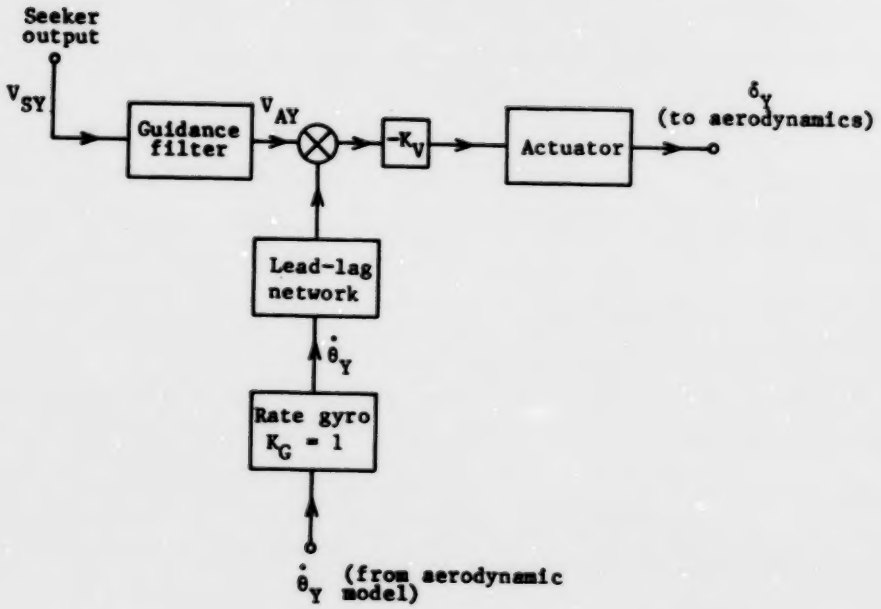

FIGURE 4 - Control of the yaw channel

2.3.2 Control-Surface Servo System

A linearized second-order actuator model (Ref. 2) is used in the simulation. One pair of control-surface servopositioners consists principally of an amplifier, a magnetic driver and a hydraulic valve actuator. Control-surface position feedback is obtained by means of a potentiometer mechanically coupled to the output shaft. The pitch and yaw channels are connected to such a pair of control-surface positioners with the phasing so arranged that the input signal will move the corresponding pair of control surfaces in the proper direction. The actuator model is given in Fig. 5. Then, the following transfer function can be derived from that figure:

$$\frac{\delta}{V_i} = \frac{K_A K_B K_C}{\tau_3 s^2 + s + K_A K_B K_C} \qquad [18]$$

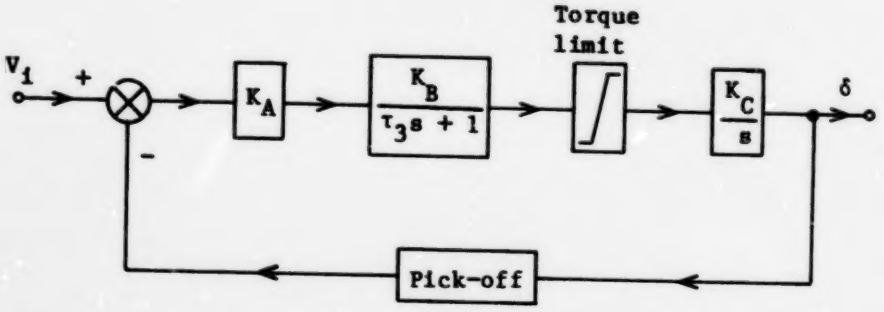

FIGURE 5 - Second-order actuator

2.3.3 Control for Body Damping

As shown in Fig. 3, the control for damping the body of the missile (Ref. 3) consists of a feedback system where the signal from a rate gyro measuring $\dot{\theta}_p$ (or $\dot{\theta}_Y$) is added to the signal at the output of the guidance filter. The resulting signal drives the actuator input. Within the loop, the gain K_V must be compensated for the variation of missile control surface effectiveness with air density at different altitudes.

This system is composed of a first-order filter to produce a phase advance and of a lead-lag network to stabilize the loop. These filters are described by the following relationship:

$$\frac{K_3\tau_6 s\ (\tau_7 s + 1)}{(\tau_8 s + 1)(\tau_9 s + 1)} \qquad [19]$$

2.3.4 Roll Stabilization

Roll stabilization is accomplished only in the pitch channel. The roll rate of the airframe $\dot{\theta}_r$ is measured by a rate gyro. Its output is then used through a lead-lag network to achieve differential movement of the control surface. The transfer function of this network is given by:

$$\frac{K_R(\tau_4 s + 1)}{(\tau_5 s + 1)} \qquad [20]$$

The use of a roll rate gyro will considerably reduce the roll rate but will not maintain the missile at a desired roll angle (Ref. 4). The channel which controls the pitch and roll orientations of the missile uses two independent fin servos, as shown in Fig. 4. Their angles, represented by δ_{PA} and δ_{PB} respectively, are combined to determine the angles δ_p and δ_R which affect the pitch and roll directions. This yields:

$$\delta_P = -\frac{1}{2}(\delta_{PA} + \delta_{PB}) \qquad [21]$$

$$\delta_R = \frac{1}{2}(\delta_{PB} - \delta_{PA}) \qquad [22]$$

The control in the yaw channel (Fig. 5) is achieved in a manner quite identical to that of the pitch channel. The difference consists in producing the same signal for the pair of control fins since this channel does not control the roll orientation of the missile.

2.4 Model of the Missile-Target Geometry

This section of the simulation consists in locating the position of the missile and target in the inertial coordinate system, and in deriving the relative velocity along each axis to yield the range and the line-of-sight rates. The following equations have been derived in Appendix C where the relative velocities along the inertial axes are given by:

$$V_X = \dot{X}_T - V_M \cos \gamma_E \cos \gamma_A \qquad [23]$$

$$V_Y = \dot{Y}_T - V_M \cos \gamma_E \sin \gamma_A \qquad [24]$$

$$V_Z = \dot{Z}_T - V_M \sin \gamma_E \qquad [25]$$

The target motion along the axes X, Y, Z is specified as either constant acceleration or constant velocity from an initial starting point. The rate of the missile velocity angles is derived from the missile-to-inertial and the body-to-missile velocity coordinate transformations, detailed in Appendix A.

$$\dot{\gamma}_E = \dot{\gamma}_P \cos \gamma_R + \dot{\gamma}_Y \sin \gamma_R \qquad [26]$$

$$\dot{\gamma}_A = (\dot{\gamma}_Y \cos \gamma_R - \dot{\gamma}_P \sin \gamma_R)/\cos \gamma_R \quad [27]$$

$$\dot{\gamma}_R = \dot{\gamma}_r - \dot{\gamma}_A \sin \gamma_E \quad [28]$$

$$\dot{\gamma}_r = \dot{\theta}_r - \dot{\theta}_p \alpha_Y + \dot{\theta}_Y \alpha_P \quad [29]$$

The range and the line-of-sight rate equations are:

$$\dot{R} = V_X \cos \sigma_A \cos \sigma_E + V_Y \sin \sigma_A \cos \sigma_E + V_Z \sin \sigma_E \quad [30]$$

$$\dot{\sigma}_A = (-V_X \sin \sigma_A + V_Y \cos \sigma_A)/R \cos \sigma_E \quad [31]$$

$$\dot{\sigma}_E = (-V_X \cos \sigma_A \sin \sigma_E - V_Y \sin \sigma_E \sin \sigma_A + V_Z \cos \sigma_E)/R \quad [32]$$

Finally, the line-of-sight rates must be transformed in the seeker-coordinate system by using the equations of Appendix A:

$$\dot{\sigma}_Y = \dot{\sigma}_A \cos \sigma_E \cos \phi_R + \dot{\sigma}_E \sin \phi_R \quad [33]$$

$$\dot{\sigma}_P = -\dot{\sigma}_A \cos \sigma_E \sin \phi_R + \dot{\sigma}_E \cos \phi_R \quad [34]$$

$\dot{\phi}_R$, the seeker rotational rate along the seeker axis X_S, is obtained by the seeker-to-inertial coordinate rotation:

$$\dot{\phi}_R = \dot{\phi}_r - \dot{\phi}_A \sin \phi_E \quad [35]$$

$$\dot{\phi}_A = (\dot{\phi}_Y \cos \phi_R - \phi_P \sin \phi_R)/\cos \phi_E \quad [36]$$

$$\dot{\phi}_E = \dot{\phi}_P \cos \phi_R + \dot{\phi}_Y \sin \phi_R \quad [37]$$

2.5 Miss Distance

The miss-distance calculation in the simulation is based on the assumption that all missile and target accelerations cease. The relative velocity vector is then projected forward to define the point of closest approach of the missile to the target. This separation is defined as the projected miss distance. The miss distance derived in Appendix C is given by:

$$MD = \frac{R^2(\dot{\sigma}_A^2 \cos^2\sigma_E + R^2\dot{\sigma}_E)^{\frac{1}{2}}}{(\dot{R}^2 + R^2\cos^2\sigma_E\dot{\sigma}_A^2 + R^2\dot{\sigma}_E^2)^{\frac{1}{2}}} \qquad [38]$$

3.0 SIMULATION OVERVIEW

The mathematical model is solved by an MPS-10 digital computer program executed on the AD-10 digital multiprocessor. This processor and its associated software are briefly described in Appendix D. The block diagram of Fig. 6 shows the simulation flowchart. Before the simulation starts, initial conditions are set and aerodynamic stability derivatives are computed as the Mach number varies from 1 to 3 in steps of 0.1 to build tables of 21 values for each of these coefficients. Atmospheric density and sound speed are also computed as the missile altitude varies from 0 to 30.5 km by steps of 242 m to build two other tables of 126 values. Gravity acceleration (g) is given as a function of the missile altitude and is contained in a table of 21 values. In addition, two dimensional tables (17 x 17 elements) are also used to represent the functions $f_1(\alpha_p, \alpha_Y)$ and $f_2(\alpha, \delta)$ of eq. 11. When the simulation runs, the stability derivatives, atmospheric density, speed of sound, gravity acceleration and functions f_1 and f_2 are extracted from the tables and a linear interpolation calculation is performed. The end of the simulation is determined by the missile-target range.

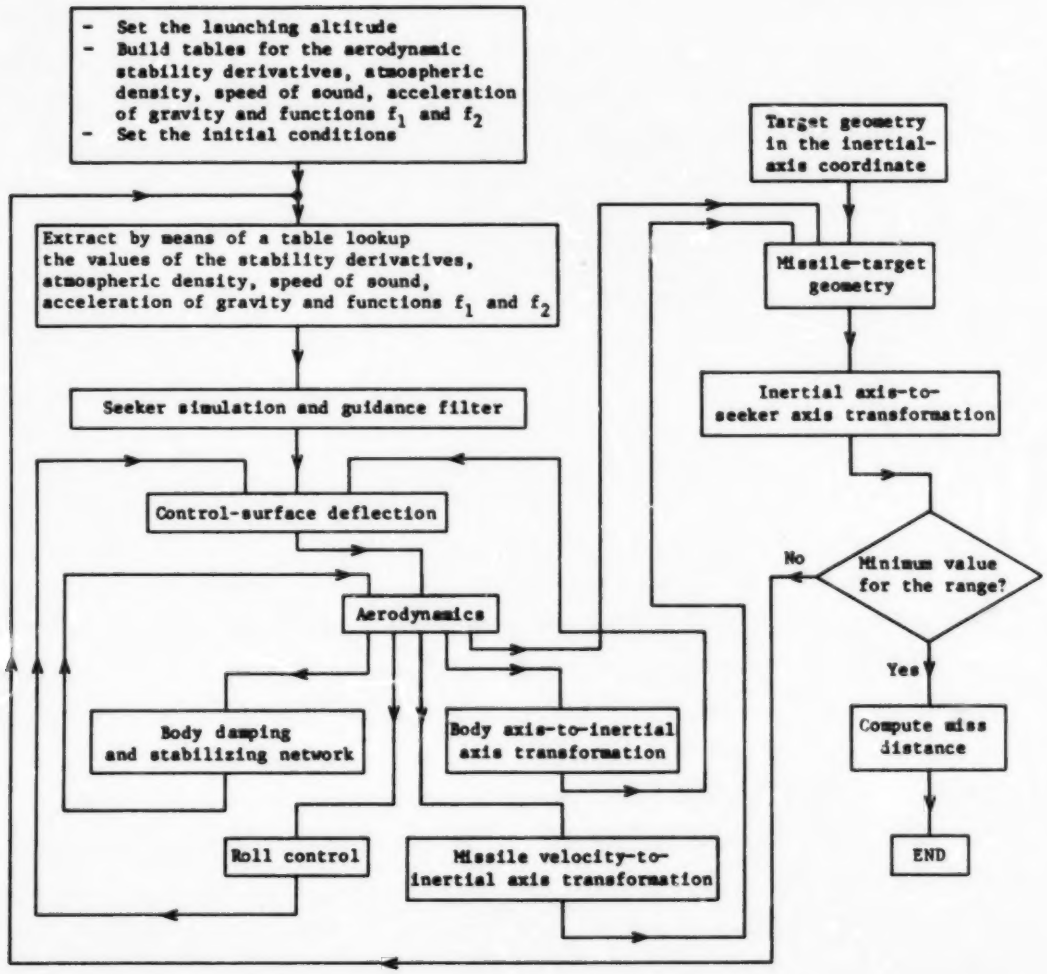
- Set the launching altitude
- Build tables for the aerodynamic stability derivatives, atmospheric density, speed of sound, acceleration of gravity and functions f_1 and f_2
- Set the initial conditions
Extract by means of a table lookup the values of the stability derivatives, atmospheric density, speed of sound, acceleration of gravity and functions f_1 and f_2
Seeker simulation and guidance filter
Control-surface deflection
Aerodynamics
Body damping and stabilizing network
Body axis-to-inertial axis transformation
Roll control
Missile velocity-to-inertial axis transformation
Target geometry in the inertial-axis coordinate
Missile-target geometry
Inertial axis-to-seeker axis transformation
Minimum value for the range?
No
Yes
Compute miss distance
END

FIGURE 6 - Block diagram of the simulation

When the range reaches a minimum value, the simulation stops and the miss distance is computed. Otherwise, the AD-10 will make another pass through all the equations.

All the integration subroutines currently available in the standard AD-10 software are executed in exactly the same length of time by the numerical integration processor (NIP) of the AD-10. Since the measure of the time required for a complete pass through all the equations of the simulation model gives 975 μs, more than 50 integration frames per cycle of the highest missile frequency f_H (which is approximately 20 Hz) are achieved by the computer. For example, using the third-order Adams-Bashforth integration method (a popular integration routine for real-time digital simulations) roughly requires 50 integration frames per cycle of f_H for a dynamic accuracy of the order of 0.1% (Ref. 5). In this case, the simulation can be run either in real time or at a speed higher than that of the actual dynamic system. Table I lists for the integration methods of the AD-10 software the maximum ratio with which the simulation can be speeded up.

TABLE I

Comparison between various integration methods as regards the maximum ratio with which the simulation can be speeded up

Integration methods	Maximum speedup factor
First-order Adams - Bashforth (AB1)	2.25
Second-order Adams - Bashforth (AB2)	2.25
Third-order Adams - Bashforth (AB3)	4.0
Fourth-order Adams - Bashforth (AB4)	2.5
Second-order Adams - Moulton (AM2)	3.2
Third-order Adams - Moulton (AM3)	3.2
Fourth-order Adams - Moulton (AM4)	2.25
Second-order Runge - Kutta (RK2)	2.25
Third-order Runge - Kutta (RK3)	5.0
Fourth-order Runge - Kutta (RK4)	3.25

4.0 SIMULATION RESULTS

To insure that the simulation operates satisfactorily, open- and closed-loop tests were performed. In the open-loop tests, the damping of the aerodynamic response and the performance of the roll control are observed when the seeker output is disconnected and step input disturbances are injected through the control system. Opening the feedback of the damping network results in an unacceptable overshoot response on the variables $\dot{\theta}$ and α, as shown in Fig. 7. When the damping system is allowed to operate, the overshoot response and oscillations on $\dot{\theta}$ and α are suppressed (Fig. 8). Tests on the roll control consist in starting the simulation with an initial roll angle rate ($\dot{\theta}_r$) of 0.5 rad/s. Without roll control, the roll angle increases from 0° to 100° in 10 s (Fig. 9). With roll control, the roll angle rate decreases from 0.5 to 0 rad/s in 4 s and the missile stops rolling (Fig. 10). The roll angle slightly oscillates with a peak amplitude smaller than 5° and it remains at 0° after the disturbance. Thus, open-loop tests verify the simulation of the aerodynamics and missile control.

Closed-loop simulations consist in presenting various missile-target encounters. Figure 11 illustrates simultaneously, in the X-Y plane, missile and target trajectories corresponding to five different scenarios. In all cases, it is assumed that the target moves at a constant speed in a direction parallel to the Y axis. The altitude of the target and its position on the X and Y axes are maintained to 12, 6.1 and 0 km respectively. The missile was launched at an altitude of 12 km and at an initial speed of 305 m/s. Initial positions of the missile on the X and Y axes coincide with the origin of these axes.

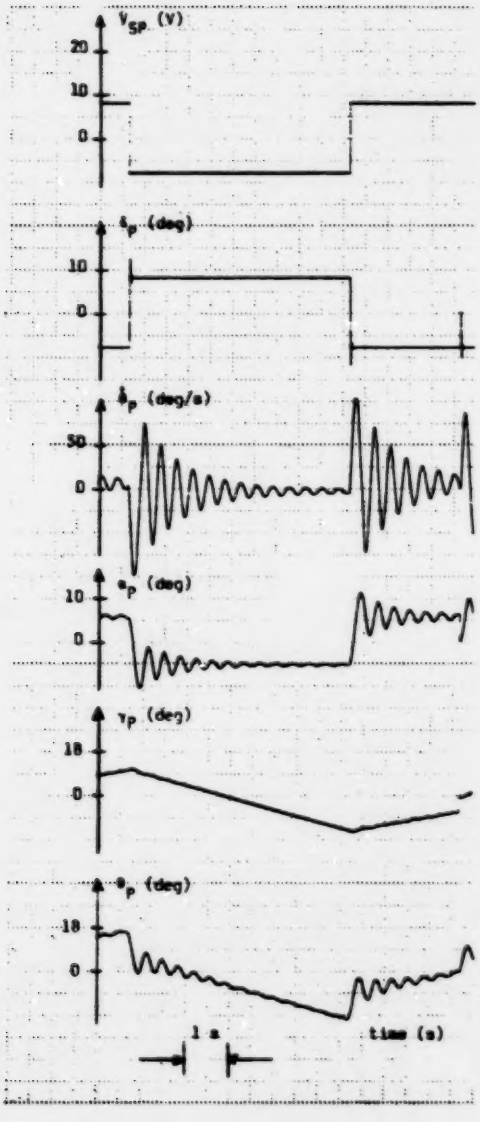

FIGURE 7 - Aerodynamic transient response without control for damping the body of the missile (Mach number = 2)

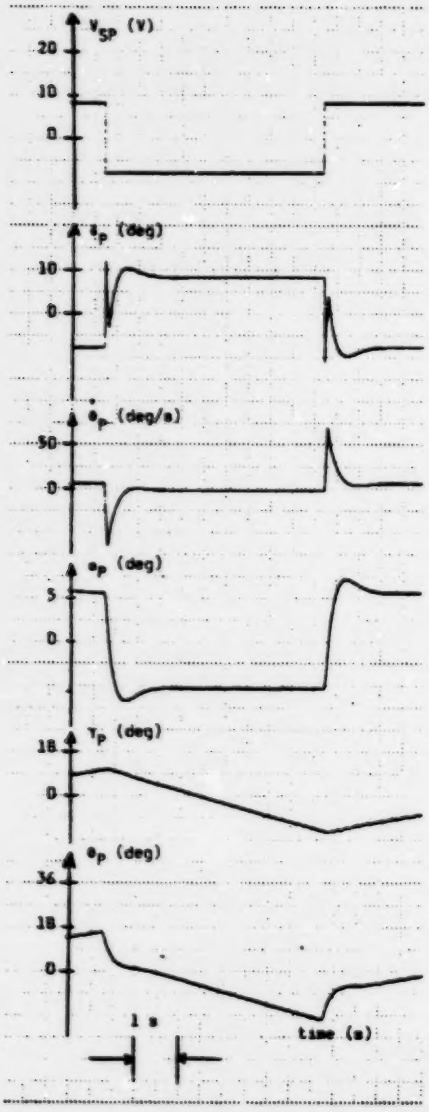

FIGURE 8 - Aerodynamic transient response with control for damping the body of the missile (Mach number = 2)

In addition, the seeker and the missile body angles are aligned along the line of sight. The trajectories were produced for target speeds of 0, 91.5, 183, 305, 366 and 396 m/s. In Fig. 12, the experiment realized previously was repeated with the following modification: the target moves at a constant speed of 488 m/s in a direction parallel and opposite to the X axis. Initial positions of the target on the X and Y axes are both adjusted to 6.1 km. Under these conditions, missile and target trajectories were produced for initial errors in the yaw plane between the line-of-sight angle (σ_Y) and the missile body angle (θ_Y) of -10°, -20°, -30° and -40°. Finally, the scenarios of Fig. 13 involve target maneuvers. As the target speed on the Y axis is kept constant at 305 m/s, the speed on the X axis, which varies as a function of time, is described by the relation $\dot{X}_T = -(152.4 + 16.94\ t^2)$ m/s. Initial positions of the target on the X and Y axes are set to 3.05 and 0 km respectively. Then, the simulation was run four times to produce missile and target trajectories which correspond to initial errors between σ_Y and θ_Y of -10°, -20°, -30° and -40°. Thus, this set of figures show typical missile trajectories where a proportional navigation guidance law is implemented in the missile.

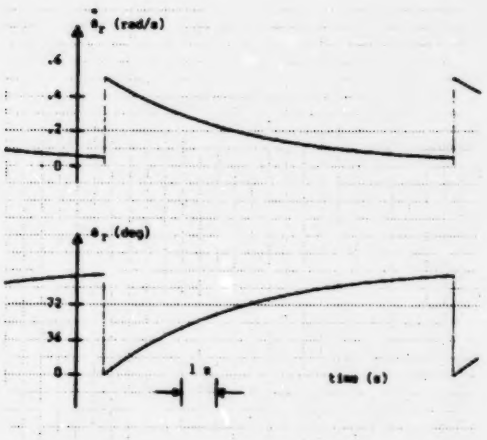

FIGURE 9 - Aerodynamic transient response without roll control (Mach number = 2)

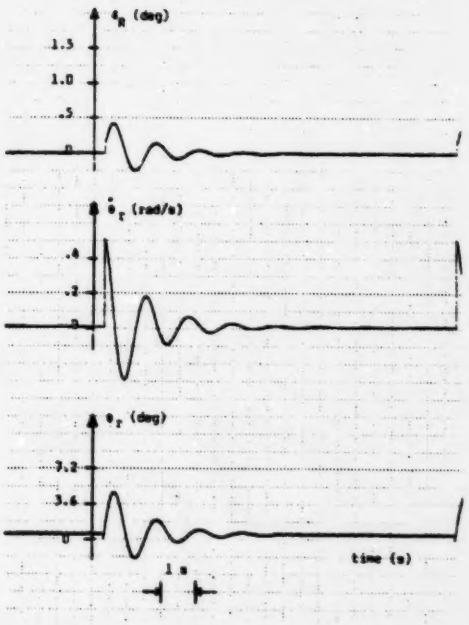

FIGURE 10 - Aerodynamic transient response with roll control (Mach number = 2)

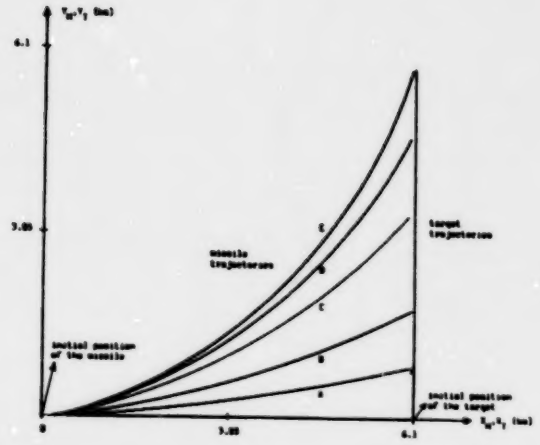

FIGURE 11 - Missile-target engagements in which the target moves in the X-Y plane at constant speeds and at a constant altitude of 12 km. The missile is launched at an altitude of 12 km at an initial speed of 305 m/s. The missile trajectories correspond to target speeds of 91.5 (Curve A), 183 (Curve B), 305 (Curve C), 366 (Curve D) and 396 m/s (Curve E)

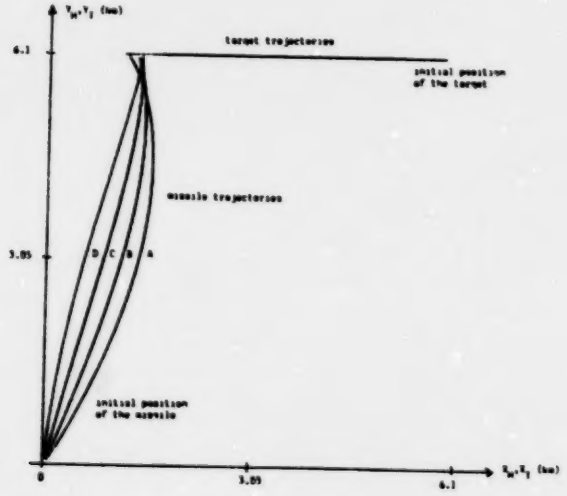

FIGURE 12 - Missile-target engagements in which the target moves in the X-Y plane at a constant speed of 488 m/s and at a constant altitude of 12 km. The missile is launched at an altitude of 12 km at an initial speed of 305 m/s. The missile trajectories correspond to initial errors between the line of sight and the missile body angles of -10° (Curve A), -20° (Curve B), -30° (Curve C) and -40° (Curve D)

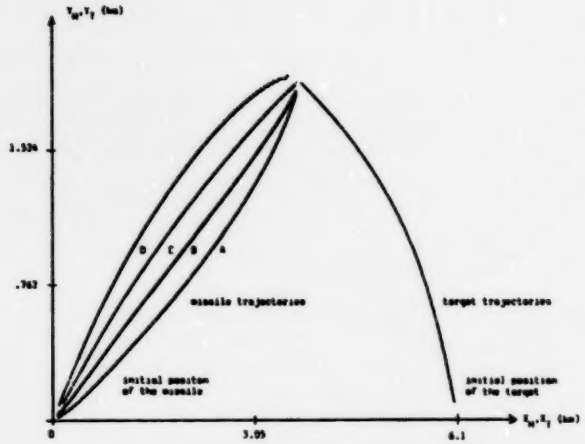

FIGURE 13 - Missile-target encounters in which the target maneuvers in the X-Y plane in maintaining a constant altitude of 12 km. The missile is launched at an altitude of 12 km at an initial speed of 305 m/s. The missile trajectories correspond to initial errors between the line of sight and the missile body angles of -10° (Curve A), -20° (Curve B), -30° (Curve C) and -40° (Curve D)

5.0 CONCLUSION

The 6 DOF missile was implemented on the AD-10 digital processor. The simulation was verified by open-loop tests carried out on the control system and by closed-loop tests in which typical missile trajectories were produced to check the operation of the guidance law of the missile. The simulation can be run in real time and, moreover, the computation speed performed by the AD-10 allows the simulation to be run faster than in real time. When the integrations are solved by the third-order Adams-Bashforth method for example, a ratio of 20 can be obtained between the time taken by the AD-10 to pass through all the equations and the smallest time constant encountered in the missile model.

The actual simulation consists of a very simplified seeker model, a linearized model of the control system involving ideal components and a linearized aerodynamic model related to small angles of attack. Since much computation time is available, a more complex model of the seeker and control could be incorporated in the simulation. These modifications would not prevent the simulation from being operated in real time. However, the most difficult problem encountered in the missile simulation is that of modeling the behavior of the seeker under all target intercept conditions. Additionally, a detailed tracking loop simulation requires modeling complex amplifier saturation characteristics and a feedback loop with very small time constants. Under this condition, rather than simulating the seeker of the missile, the actual simulation could be in interaction with the seeker hardware.

The missile simulation can be applied to other types of missiles. The aerodynamic model is adequate for the majority of guided missiles. In addition, target-missile kinematic and coordinate system transformations would not be modified at all. However, other control systems and autopilot arrangements different from those presented in this report can be used. For example, some missiles use canards or moving wings and missile stability is achieved by position gyroscopes, accelerometers or aerodynamic rollerons.

6.0 REFERENCES

1. Carpentier, R., "Guidage des Avions et des Missiles Aérodynamiques", Ecole Nationale Supérieure de l'Aéronautique et de l'Espace, Paris, 1973.

2. Pastrick, H.L., York, R.J. and Jolly, A.C., "System Performance Prediction by Modelling Test Data in Digital Simulation", Paper 73-880 of AIAA Guidance and Control Conference, Key Biscayne, Florida, 1973.

3. Garnell, P. and East, D.J., "Guided Weapons Control System", Pergamon Press, London, 1975.

4. Blakelock, J.H., "Automatic Control of Aircraft and Missiles", John Wiley & Sons, Inc., New York, 1965.

5. "Application of the AD-10 to Six-Degrees-of-Freedom Flight Equations", Applied Dynamic International, Ann Arbour, Michigan, 1980.

APPENDIX A

Coordinate Systems and Coordinate Systems Rotations

A.1 Coordinate Systems

Five coordinate systems are used in the simulation. One is the earth-fixed coordinate system (X, Y, Z); the other four, (X_B, Y_B, Z_B), (X_L, Y_L, Z_L), (X_S, Y_S, Z_S) and (X_V, Y_V, Z_V), are identified as the body-, the line-of-sight-, the seeker- and the missile-velocity coordinate systems.

Missile-target geometric relationships are computed in the earth-fixed coordinate system illustrated in Fig. A1. The Z axis is defined to be parallel and opposite to the gravity vector. This axis is perpendicular to the X-Y plane such that the X, Y, and Z axes form a right-handed system. The axis system XYZ is fixed with respect to the earth and is considered inertial.

The body-coordinate system is shown in Fig. A2. The origin is located at the missile center of gravity. The X_B axis lies in the forward direction along the missile centerline. Assuming the missile is in a zero roll orientation, the Z_B axis is perpendicular to the plane formed by the fins which cause motion in the pitch plane, i.e. in the "up/down" direction. The Y_B axis lies in the yaw or right-left plane such that the X_B, Y_B, Z_B axes form a right-handed system. The pitch and yaw notation is used extensively in the simulation to signify the (X_B, Z_B) and the (X_B, Y_B) planes respectively.

The seeker-coordinate system (X_S, Y_S, Z_S) is shown in Fig. A3. If the head gyro spin axis is along the missile centerline, the seeker- and body-coordinate systems coincide. Rotations about the Y_B and Z_S axes, through the angles λ_Y and λ_P, define the seeker coordinate

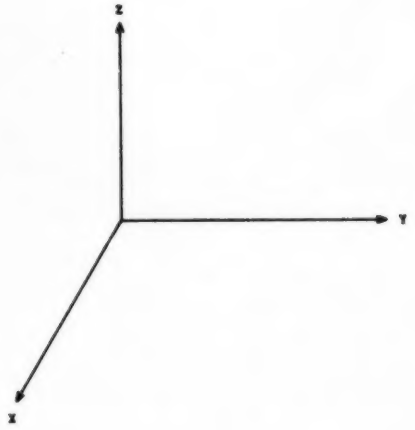

FIGURE A1 - Stationary coordinate system (XYZ)

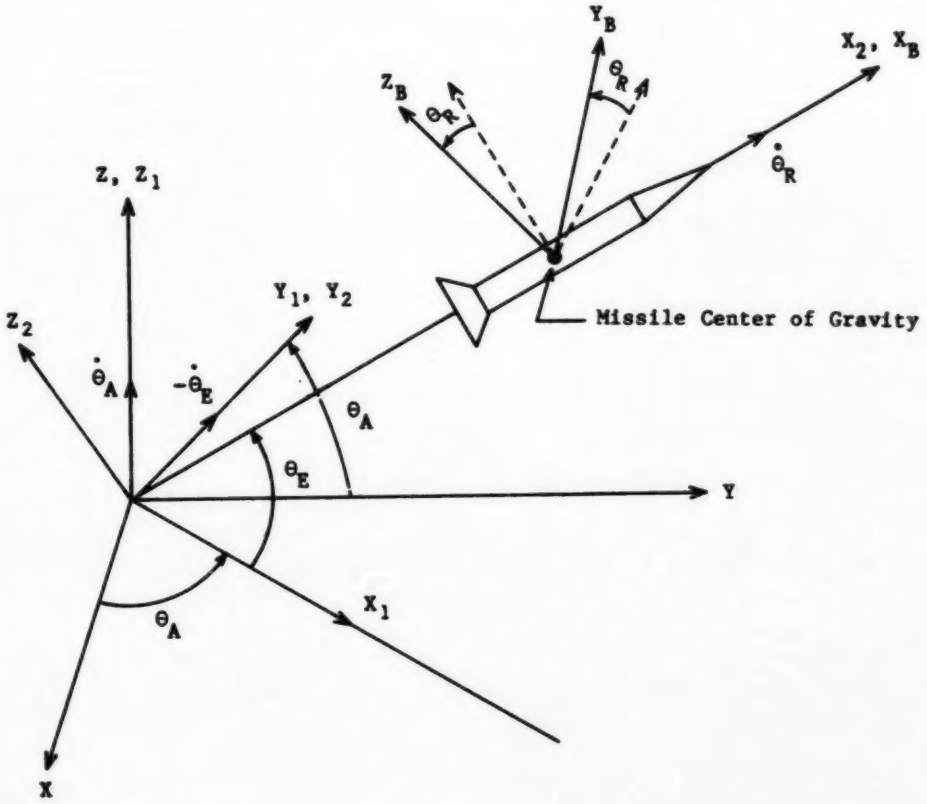

FIGURE A2 - Body-coordinate system (X_B, Y_B, Z_B)

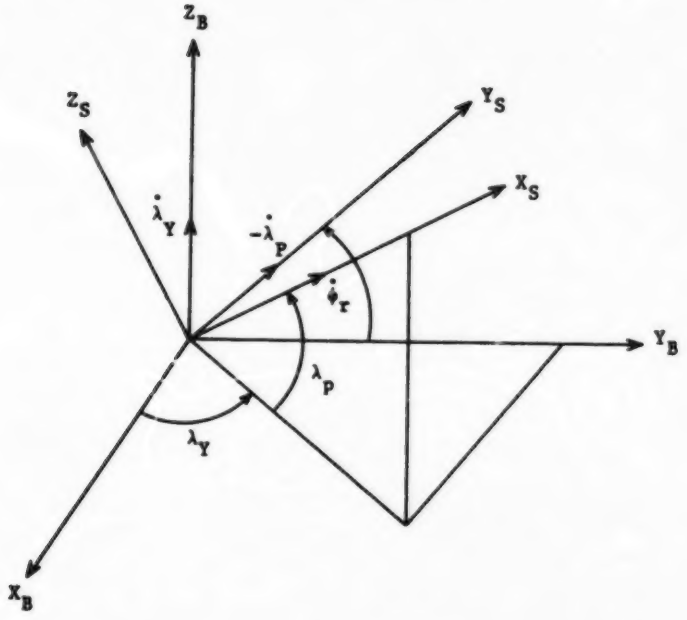

FIGURE A3 - Seeker-coordinate system (X_S, Y_S, Z_S)

system, with the X_S axis aligned with the gyro spin axis. Note that the assumption is made that the origins of the body- and the seeker-coordinate systems coincide.

A fourth coordinate system is illustrated in Fig. A4. The X_L axis is defined as being parallel to the range vector; i.e, along the line of sight from the missile (M) to the target (T). Referencing this system to the stationary coordinate system, azimuth and elevation rotations about the Z and Y_L axes through the angles σ_A and σ_E define the orientation of the line-of-sight axes.

The fifth coordinate system (X_V, Y_V, Z_V) used in the simulation is the missile velocity coordinate system shown in Fig. A5. Angles-of-attack rotations about the Z_B and the Y_V axes through the angles α_Y and α_P define the orientation of the missile velocity axes.

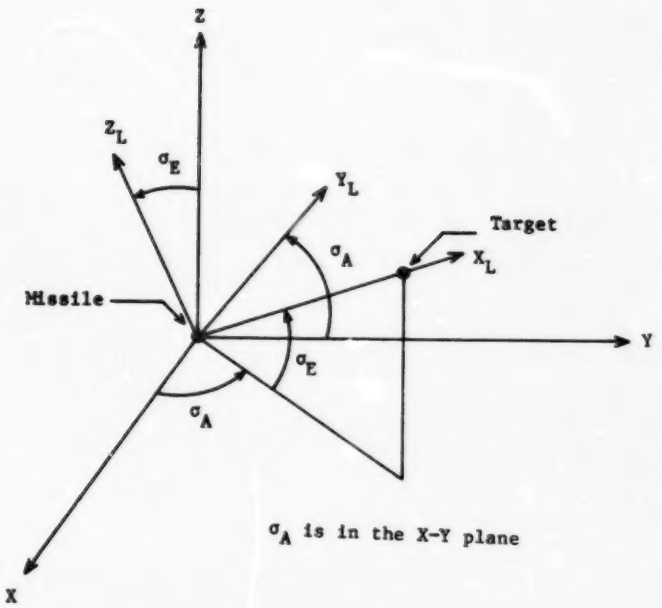

FIGURE A4 - Line-of-sight coordinate system (X_L, Y_L, Z_L)

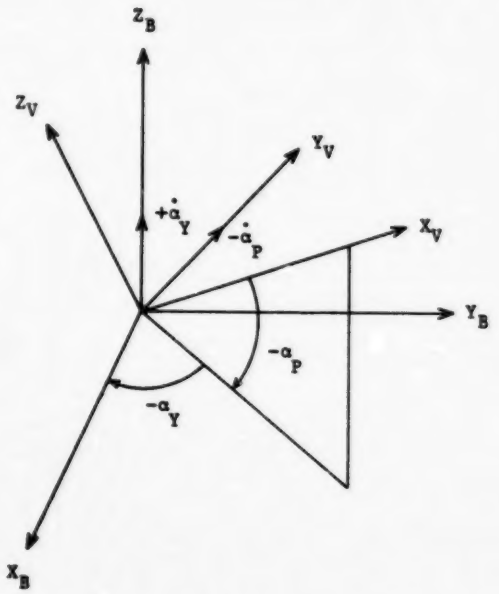

FIGURE A5 - Missile-velocity coordinate system (X_V, Y_V, Z_V)

A.2 Coordinate System Rotation

A.2.1 Body-to-Inertial Coordinate Rotation

Euler angles are used to define the orientation of the body axes relative to the stationary axes. The simulation defines the Euler rotation as θ_A, θ_E and θ_R. The orientation of body axes, after successive rotation through θ_A, θ_E and θ_R, is shown in Fig. A2. Defining (i, j, k) as the unit vector in the body system and (i_B, j_B and k_B) as the unit vector along the body system, the following transformation matrices hold between coordinate systems:

$$\begin{bmatrix} i \\ j \\ k \end{bmatrix} = \begin{bmatrix} \cos\theta_A & -\sin\theta_A & 0 \\ \sin\theta_A & \cos\theta_A & 0 \\ 0 & 0 & 1 \end{bmatrix} \begin{bmatrix} i_1 \\ j_1 \\ k_1 \end{bmatrix} \qquad [A.1]$$

$$\begin{bmatrix} i_1 \\ j_1 \\ k_1 \end{bmatrix} = \begin{bmatrix} \cos\theta_E & 0 & -\sin\theta_E \\ 0 & 1 & 0 \\ \sin\theta_E & 0 & \cos\theta_E \end{bmatrix} \begin{bmatrix} i_2 \\ j_2 \\ k_2 \end{bmatrix} \qquad [A.2]$$

$$\begin{bmatrix} i_2 \\ j_2 \\ k_2 \end{bmatrix} = \begin{bmatrix} 1 & 0 & 0 \\ 0 & \cos\theta_R & -\sin\theta_R \\ 0 & \sin\theta_R & \cos\theta_R \end{bmatrix} \begin{bmatrix} i_B \\ j_B \\ k_B \end{bmatrix} \qquad [A.3]$$

The angular rotation of the body-coordinate system is defined in the earth system as:

$$\omega = \dot{\theta}_R \, i_B - \dot{\theta}_A \, j + \dot{\theta}_E k_1 \qquad [A.4]$$

where a dot above a variable indicates the derivative of the variable with respect to time. Similarly, the body rotation expressed in the body-coordinate system is defined as:

$$\omega = \dot{\theta}_r \, i_B - \dot{\theta}_P j_B + \dot{\theta}_y k_B \qquad [A.5]$$

Transforming eq. A.4 by using the coordinate transformations in eqs. A.1 to A.3 and equating components of identical unit vectors in eq. A.5 yield:

$$\dot{\theta}_E = \dot{\theta}_P \cos \theta_R + \dot{\theta}_Y \sin \theta_R \qquad [A.6]$$

$$\dot{\theta}_A = (\dot{\theta}_Y \cos \theta_R - \dot{\theta}_P \sin \theta_R)/\cos \theta_E \qquad [A.7]$$

$$\dot{\theta}_R = \dot{\theta}_r - \dot{\theta}_A \sin \theta_E \qquad [A.8]$$

Equations A.6 to A.8 describe the angular orientation of the missile-body coordinate system relative to the stationary coordinate system as a function of the airframe rates expressed in the body system. These rates ($\dot{\theta}_Y$, $\dot{\theta}_P$, $\dot{\theta}_r$) are determined by considering the external forces and moments acting on the airframe, and are derived in equations of motion herein.

A.2.2 Seeker-to-Inertial Coordinate Rotation

The orientation of the seeker coordinate system relative to the stationary coordinate system is determined in a manner identical to that of the body Euler angles. The seeker angles in the inertial axes are represented by the three Euler angles ϕ_A, ϕ_E and ϕ_R. Defining i_S, j_S and k_S as unit vectors along the seeker axes X_S, Y_S and Z_S, the angular rotation of the seeker coordinate system is defined in the stationary system as:

$$\omega_S = \dot{\phi}_r i_S - \dot{\phi}_P j_S + \dot{\phi}_Y k_S \qquad [A.9]$$

By resolving seeker rotational rates into the inertial-axis system, the following equations are obtained:

$$\dot{\phi}_E = \dot{\phi}_P \cos \phi_R + \dot{\phi}_Y \sin \phi_R \qquad [A.10]$$

$$\dot{\phi}_A = (\dot{\phi}_Y \cos \phi_R - \dot{\phi}_P \sin \phi_R)/\cos \phi_E \qquad [A.11]$$

$$\dot{\phi}_R = \dot{\phi}_r - \dot{\phi}_A \sin \phi_E \qquad [A.12]$$

A.2.3 Seeker-to-Body Coordinate Rotation

The angular rate of the seeker ω_S can be expressed in terms of the body angular rate ω_B and the relative rate $\omega_{S/B}$ as:

$$\omega_S = \omega_{S/B} + \omega_B \qquad [A.13]$$

where

$$\omega_B = \dot{\theta}_r i_B - \dot{\theta}_P j_B + \dot{\theta}_Y k_B \qquad [A.14]$$

$$\omega_S = \dot{\phi}_r i_S - \dot{\phi}_P j_S + \dot{\phi}_Y k_S \qquad [A.15]$$

$$\omega_{S/B} = -\dot{\lambda}_P y_S + \dot{\lambda}_Y k_B \qquad [A.16]$$

The expressions for $\dot{\lambda}_P$, $\dot{\lambda}_Y$ and $\dot{\phi}_r$ define the seeker-coordinate system motion relative to the body. The body-unit vectors expressed in terms of a transformation of the seeker-unit vectors are given by:

$$\begin{bmatrix} i_B \\ j_B \\ k_B \end{bmatrix} = \begin{bmatrix} \cos\lambda_Y\cos\lambda_P & -\sin\lambda_Y & -\cos\lambda_Y\sin\lambda_P \\ \sin\lambda_Y\cos\lambda_P & \cos\lambda_Y & -\sin\lambda_P\sin\lambda_Y \\ \sin\lambda_P & 0 & \cos\lambda_P \end{bmatrix} \begin{bmatrix} i_S \\ j_S \\ k_S \end{bmatrix} \qquad [A.17]$$

Converting eq. A.13 into the seeker-unit vector and equating unit-vector components yield:

$$\dot{\phi}_r = \sin\lambda_P(\dot{\lambda}_Y + \dot{\theta}_Y) + \dot{\theta}_r\cos\lambda_Y\cos\lambda_P + \dot{\theta}_P\sin\lambda_Y\cos\lambda_P \qquad [A.18]$$

$$\dot{\lambda}_P = \dot{\phi}_P + \dot{\theta}_r\sin\lambda_Y - \dot{\theta}_P\cos\lambda_Y \qquad [A.19]$$

$$\dot{\lambda}_Y = (\dot{\phi}_Y + \dot{\theta}_r\cos\lambda_Y\sin\lambda_P + \dot{\theta}_P\sin\lambda_P\sin\lambda_Y - \dot{\theta}_Y\cos\lambda_P)/\cos\lambda_P \qquad [A.20]$$

A.2.4 Inertial-to-Seeker and Seeker-to-Line-of-Sight Coordinate Rotation

The inertial-to-seeker coordinate transformation of the line-of-sight rates, $\dot{\sigma}_A$ and $\dot{\sigma}_E$, is derived in a manner identical to that of the derivation of the transformation of the seeker rates $\dot{\phi}_A$ and $\dot{\phi}_E$. Taking the inverse of the transformation of eqs. A.10 and A.11 by substituting $\dot{\phi}$ by $\dot{\sigma}$, the pitch and yaw line-of-sight rate components as sensed by the seeker are:

$$\dot{\sigma}_Y = \dot{\sigma}_A \cos \sigma_E \cos\phi_R + \dot{\sigma}_E \sin \phi_R \qquad [A.21]$$

$$\dot{\sigma}_P = -\dot{\sigma}_A \cos \sigma_E \sin \phi_R + \dot{\sigma}_E \cos \phi_R \qquad [A.22]$$

Figure A6 illustrates graphically the relation between the line-of-sight vector and the gyro spin axis. The optical system senses the angular separation ε between the line of sight to the target and the gyro spin axis. The seeker signal processing generates a current in the gyro precession coils resulting in a precession rate, $\dot{\phi}$, proportional to this error.

The tracking rate of the gyro is dependent on the magnitude of the error in the pitch and yaw channels. The expressions for these angular separations can be derived in a manner similar to that of the derivation of seeker-to-body coordinate relations of eqs. A.13 to A.20.

The angular rate of the line-of-sight vector in relation to the seeker angular rate is given by:

$$\omega_{LOS/S} = \omega_{LOS} - \omega_S \qquad [A.23]$$

where

$$\omega_{LOS/S} = -\dot{\varepsilon}_P j_L + \dot{\varepsilon}_Y k_S \qquad [A.24]$$

$$\omega_{LOS} = -\dot{\sigma}_P j_L + \dot{\sigma}_Y k_L \qquad [A.25]$$

$$\omega_S = \dot{\phi}_r i_S - \phi_P j_S + \dot{\phi}_Y k_S \qquad [A.26]$$

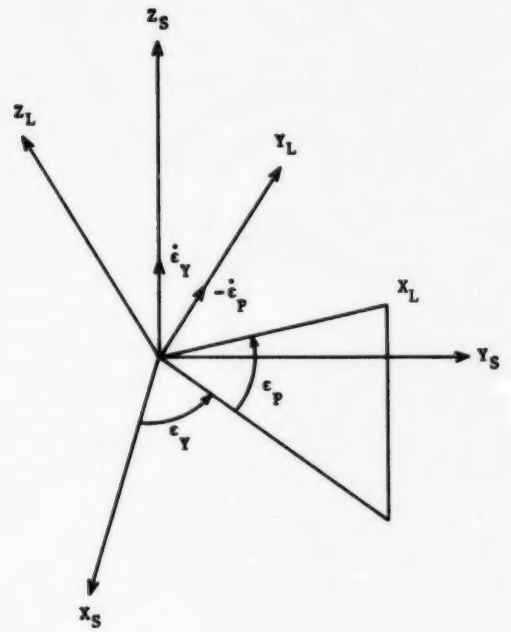

FIGURE A6 - Line-of-sight vector orientation

Substituting in eq. A.23 the seeker-to-line-of-sight coordinate transformation given by:

$$\begin{bmatrix} i_S \\ f_S \\ k_S \end{bmatrix} = \begin{bmatrix} \cos\epsilon_Y\cos\epsilon_P & -\sin\epsilon_Y & -\cos\epsilon_Y\sin\epsilon_P \\ \sin\epsilon_Y\cos\epsilon_P & \cos\epsilon_Y & -\sin\epsilon_Y\sin\epsilon_P \\ \sin\epsilon_P & 0 & \cos\epsilon_P \end{bmatrix} \begin{bmatrix} i_L \\ f_L \\ k_L \end{bmatrix} \qquad [A.27]$$

and equating components of the identical unit vector yield:

$$\dot{\epsilon}_P = \dot{\sigma}_P - \dot{\phi}_P \cos\epsilon_Y - \dot{\phi}_r \sin\epsilon_Y \qquad [A.28]$$

$$\dot{\varepsilon}_Y = (\dot{\sigma}_Y - \dot{\phi}_Y \cos\varepsilon_P + \dot{\phi}_r \cos\varepsilon_Y \sin\varepsilon_P - \dot{\phi}_P \sin\varepsilon_Y \sin\varepsilon_P)/\cos\varepsilon_P \quad [A.29]$$

Since the maximum angular separation ε is considerably less than 10°, small angle approximations may be used to simplify the error equations to:

$$\dot{\varepsilon}_P = \dot{\sigma}_P - \dot{\phi}_P - \dot{\phi}_r \varepsilon_Y \quad [A.30]$$

$$\dot{\varepsilon}_Y = \dot{\sigma}_Y - \dot{\phi}_Y + \dot{\phi}_r \varepsilon_P \quad [A.31]$$

A.2.5 Body-to-Missile Velocity Coordinate Rotation

The orientation of the velocity-coordinate system is given by:

$$\omega_V = \dot{\gamma}_r i_V - \dot{\gamma}_P j_V + \dot{\gamma}_Y K_V \quad [A.32]$$

where i_V, j_V and k_V are unit vectors along the (X_V, Y_V, Z_V) axes. By resolving velocity rotational rates into the stationary axis system, the following equations for Euler angles are obtained:

$$\dot{\gamma}_E = \dot{\gamma}_P \cos\gamma_R + \dot{\gamma}_Y \sin\gamma_R \quad [A.33]$$

$$\dot{\gamma}_A = (\dot{\gamma}_Y \cos\gamma_R - \dot{\gamma}_P \sin\gamma_R)/\cos\gamma_E \quad [A.34]$$

$$\dot{\gamma}_R = \dot{\gamma}_r - \dot{\gamma}_A \sin\gamma_E \quad [A.35]$$

The angular rotation of the velocity-coordinate system, in terms of the body angular rates ω_B and the relative rate $\omega_{B/V}$, is:

$$\omega_V = \omega_B - \omega_{B/V} \quad [A.36]$$

where

$$\omega_{B/V} = -\dot{\alpha}_P j_V + \dot{\alpha}_Y K_B$$

Using the body-to-velocity axis transformation given by:

$$\begin{bmatrix} i_B \\ j_B \\ k_B \end{bmatrix} = \begin{bmatrix} \cos\alpha_Y\cos\alpha_P & -\sin\alpha_Y & -\cos\alpha_Y\sin\alpha_P \\ \sin\alpha_Y\cos\alpha_P & \cos\alpha_Y & -\sin\alpha_P\sin\alpha_Y \\ \sin\alpha_P & 0 & \cos\alpha_P \end{bmatrix} \begin{bmatrix} i_V \\ j_V \\ k_V \end{bmatrix}$$

converting eq. A.36 into velocity-unit vectors and equating unit-vector components yield:

$$\dot{\gamma}_r = \dot{\theta}_r\cos\alpha_Y\cos\alpha_P - \dot{\theta}_P\sin\alpha_Y\cos\alpha_P + \dot{\theta}_Y\sin\alpha_P - \alpha_Y\sin\alpha_P \quad [A.38]$$

$$\dot{\gamma}_P = -\dot{\alpha}_P + \dot{\theta}_r\sin\alpha_Y + \dot{\theta}_P\cos\alpha_Y \quad [A.39]$$

$$\dot{\gamma}_Y = \dot{\alpha}_Y\cos\alpha_P - \dot{\theta}_r\cos\alpha_Y\sin\alpha_P + \dot{\theta}_P\sin\alpha_P\sin\alpha_Y + \dot{\theta}_Y\cos\alpha_P \quad [A.40]$$

Small angle approximation on angles α_P and α_Y leads to the relations:

$$\dot{\gamma}_r = \dot{\theta}_r - \dot{\theta}_P\alpha_Y + \dot{\theta}_Y\alpha_P - \dot{\alpha}_Y\alpha_P \quad [A.41]$$

$$\dot{\gamma}_P = -\dot{\alpha}_P + \dot{\theta}_r\alpha_Y + \dot{\theta}_P \quad [A.42]$$

$$\dot{\gamma}_Y = -\dot{\alpha}_Y - \dot{\theta}_r\alpha_P + \dot{\theta}_Y \quad [A.43]$$

which are used to compute the velocity vector angles.

APPENDIX B

Missile Aerodynamics

The translation and rotation of the body axes (X_B, Y_B, Z_B) form the six degrees of freedom that describe the missile motion. The equations used in the simulation are derived from the classical Euler vector equations of motion for rigid bodies relating forces ($\vec{F}$), velocity ($\vec{V}$), moment ($\vec{M}$) and angular momentum ($\vec{H}$). These equations, which constitute textbook material of Refs. 1, 3, 4, 5 and B1, are:

$$\vec{F} = m \frac{d\vec{V}_M}{dt} + m\vec{\omega}_M \times \vec{V}_M \qquad [B.1]$$

$$\vec{M} = \frac{d\vec{H}}{dt} + \vec{\omega} \times \vec{H} \qquad [B.2]$$

where

$$\vec{V}_M = u\vec{i}_B + v\vec{j}_B + w\vec{k}_B \qquad [B.3]$$

$$\vec{\omega}_M = \dot{\theta}_r\vec{i}_B - \dot{\theta}_p\vec{j}_B + \dot{\theta}_Y\vec{k}_B \qquad [B.4]$$

$$\vec{H} = I_X\dot{\theta}_r\vec{i}_B - I_Y\dot{\theta}_P\vec{j}_B + I_Z\dot{\theta}_Y\vec{k}_B \qquad [B.5]$$

In eqs. B.4 and B.5, it is assumed that the missile is cruciform, i.e. a symmetry exists about the $X_B - Z_B$ and the $X_B - Y_B$ axes. Therefore, all the products of inertia terms are zero and $I_Y = I_Z$.

The scalar components of eqs. B.1 and B.2 are

$$F_X = m(\dot{u} - \dot{\theta}_P w - \dot{\theta}_Y v) \qquad [B.6]$$

$$F_Y = m(\dot{v} + \dot{\theta}_Y u - \dot{\theta}_r w) \qquad [B.7]$$

$$F_Z = m(\dot{w} + \dot{\theta}_P u + \dot{\theta}_r v) \qquad [B.8]$$

$$M_X = I_X \ddot{\theta}_r \qquad [B.9]$$

$$M_Y = I_Y \ddot{\theta}_P + (I_X - I_Z)\, \dot{\theta}_Y \dot{\theta}_r \qquad [B.10]$$

$$M_Z = I_Z \ddot{\theta}_Y + (I_Y - I_X)\dot{\theta}_P \dot{\theta}_r \qquad [B.11]$$

The translational equations of motion are determined by the sum of external forces and moments applied to the airframe. The forces modeled in the simulation are propulsion, gravity and aerodynamic forces. The aerodynamic force and moment coefficients vary as functions of Mach number, angle of attack, surface control and roll orientation. These relationships are modeled using partial derivates in nonlinear algebraic equations:

$$F_X = T - qS(C_{D0} + C_{D\alpha^2}(\alpha_P^2 + \alpha_Y^2) - mg \sin \theta_E \qquad [B.12]$$

$$F_Y = qS(C_{L\alpha}\alpha_Y + C_{L\delta}\delta_Y) - mg \cos\theta_E \sin\theta_R \qquad [B.13]$$

$$F_Z = qS(C_{L\alpha}\alpha_P + C_{L\delta}\delta_P) - mg \cos\theta_E \cos\theta_R \qquad [B.14]$$

The aerodynamic moments are:

$$M_X = -qSd\ (C_{\ell\delta}\delta_R + \frac{d}{V_M} C_{\ell\dot{\theta}}\dot{\theta}_R + f_1(\alpha_P, \alpha_Y) C_{\ell\alpha_P\alpha_Y} + f_2(\alpha, \delta)\ C_{\ell\alpha\delta}) \qquad [B.15]$$

$$M_Y = -qSd(C_{m\alpha}\alpha_P + C_{m\delta}\delta_P + \frac{d}{V_M}(C_{m\dot{\theta}}\dot{\theta}_P)) \qquad [B.16]$$

$$M_Z = -qSd(C_{m\alpha}\alpha_Y + C_{m\delta}\delta_Y + \frac{d}{V_M}(C_{m\dot{\theta}}\dot{\theta}_Y)) \qquad [B.17]$$

where q, the dynamic pressure, is equal to $\rho V_M^2/2$. Equations B.12 to B.17 have been derived for a cruciform configuration in which the maneuvering control is located at the rear of the missile. We assume also that the second-order coefficients ($C_{D\delta}{}^2$, $C_{D\alpha\delta}$, $C_{m\alpha\delta}$, $C_{m\alpha}{}^2$) and the dynamic coefficient $C_{m\dot{\alpha}}$ are negligible.

The translation equation can be combined to extract the magnitude of the missile velocity and its angular velocity in the pitch and yaw planes, $\dot{\gamma}_P$ and $\dot{\gamma}_Y$, respectively.

The magnitude of the missile velocity is given by:

$$V_M = (u^2 + v^2 + w^2)^{\frac{1}{2}} \qquad [B.18]$$

Differentiating eq. B.18:

$$\dot{V}_M = \frac{u}{V_M}\dot{u} + \frac{v}{V_M}\dot{v} + \frac{w}{V_M}\dot{w} \qquad [B.19]$$

and substituting eqs. B.6 to B.9 in B.19 yield:

$$m\dot{V}_M = \frac{u}{V_M}F_X + \frac{v}{V_M}F_Y + \frac{w}{V_M}F_Z \qquad [B.20]$$

From Fig. A5, the following relations between the velocity V_M and its components (u, v, w) along the body axes hold:

$$u = V_M \cos\alpha_Y \cos\alpha_P \qquad [B.21]$$

$$v = - V_M \cos\alpha_P \sin\alpha_Y \qquad [B.22]$$

$$w = - V_M \sin\alpha_P \qquad [B.23]$$

If we assume that the components of the angle of attack (α_P, α_Y) do not exceed 20°, small angle approximations of eqs. B.21 to B.23 give:

$$u \approx V_M \qquad [B.24]$$

$$v \approx -V_M \alpha_Y \qquad [B.25]$$

$$w \approx -V_M \alpha_P \qquad [B.26]$$

Substituting eqs. B.24 to B.26 in eq. B.20 yields:

$$\dot{V}_M = \frac{F_X}{m} - \frac{F_Y \alpha_Y}{m} - \frac{F_Z \alpha_P}{m} \qquad [B.27]$$

The angular variation of the missile velocity in the pitch plane is obtained by first differentiating eq. B.26:

$$\dot{\alpha}_P = \frac{w\dot{V}_M - \dot{w}V_M}{V_M^2} \qquad [B.28]$$

and substituting eqs. B.6 to B.8 and B.24 to B.27 in eq. B.28 to give:

$$\dot{\alpha}_P = \dot{\theta}_P - \frac{F_X \alpha_P}{mV_M} - \frac{F_Z}{mV_M} + \dot{\theta}_r \alpha_Y - \frac{F_Z w^2}{mV_M^3} - \frac{F_Y vw}{mV_M^3} \qquad [B.29]$$

Assuming that $F_Y vw/mV^3$ and $F_Z w^2/mV^3$ are negligible and substituting eq. A.42 in eq. B.29 yield:

$$\dot{\gamma}_P = \frac{F_X \alpha_P}{mV_M} + \frac{F_Z}{mV_M} \qquad [B.30]$$

Similarly, the same procedure applied to the yaw plane, for small $F_Y v^2/mV_M^3$ and $F_Z vw/mV_M^3$ and for $\dot{\alpha}_Y$ substituted by the relation of eq. A.43, leads to:

$$\dot{\gamma}_Y = \frac{F_X \alpha_Y}{mV_M} + \frac{F_Y}{mV_M} \qquad [B.31]$$

Finally, if we replace the external forces and moments of eqs. B.12 to B.17 in eqs. B.30, B.37 and B.15 to B.17, the airframe model becomes:

$$\dot{V}_M = (F_X - F_Y \alpha_Y - F_Z \alpha_P)/m \qquad [B.32]$$

$$\dot{\gamma}_P = \frac{qS}{mV_M} (C_{L\alpha} \alpha_P + C_{L\delta} \delta_P + \frac{F_X \alpha_P}{mV_M} - \frac{g}{V_M} \cos\theta_E \cos\theta_R) \qquad [B.33]$$

$$\dot{\gamma}_Y = \frac{qS}{mV_M} (C_{L\alpha} \alpha_Y + C_{L\delta} \delta_Y + \frac{F_X \alpha_Y}{mV_M} - \frac{g}{V_M} \cos\theta_E \sin\theta_R) \qquad [B.34]$$

$$\ddot{\theta}_P = - \frac{qSd}{I_Y} [C_{m\alpha} \alpha_P + C_{m\delta} \delta_P + \frac{d}{V_M} (C_{m\dot{\theta}} \dot{\theta}_P)] - \frac{(I_X - I_Z)}{I_Y} \dot{\theta}_Y \dot{\theta}_r \qquad [B.35]$$

$$\ddot{\theta}_Y = - \frac{qSd}{I_Z} [C_{m\alpha} \alpha_Y + C_{m\delta} \delta_Y + \frac{d}{V_M} (C_{m\dot{\theta}} \dot{\theta}_P)] - \frac{(I_Y - I_X)}{I_Z} \dot{\theta}_P \dot{\theta}_r \qquad [B.36]$$

$$\ddot{\theta}_R = - \frac{qSd}{I_X} [C_{\ell\delta} \delta_R + f_1(\alpha_P, \alpha_Y) C_{\ell\alpha\alpha} + f_2(\alpha, \delta) C_{\ell\alpha\delta} + \frac{d}{V_M} C_{\ell\dot{\theta}} \dot{\theta}_R] \qquad [B.37]$$

For the present model, speed of sound and atmospheric density are approximated by the following equations:

$$V_s = 340.24\ [1 - 2.256 \times 10^{-5} Z_M]^{\frac{1}{2}}\ \text{m/s} \qquad [B.38]$$

$$\rho = .4677[1 - 2.256 \times 10^{-5} Z_M]^{4.258}\ \text{Kg/m}^3 \qquad [B.39]$$

if the altitude is smaller than 10.772 km, and

$$V_s = 296\ \text{m/s}$$

$$\rho = .143 \exp[-4.778 \times 10^{-5}(3.28\ Z_M - 35{,}332)]\ \text{kg/m}^3$$

if the altitude is greater than 10.772 km.

REFERENCE

B1. Etkin, B., "Dynamics of Atmospheric Flight", John Wiley & Sons, Inc., New York, 1972.

APPENDIX C

Missile-Target Geometry

Rotation of the line-of-sight axes into the stationary axes is described by the following transformation:

$$\begin{bmatrix} i \\ j \\ k \end{bmatrix} = \begin{bmatrix} \cos\sigma_A\cos\sigma_E - \sin\sigma_A & -\cos\sigma_A\sin\sigma_E \\ \sin\sigma_A\cos\sigma_E \quad \cos\sigma_A & -\sin\sigma_E\sin\sigma_A \\ \sin\sigma_E \quad 0 \quad \cos\sigma_E \end{bmatrix} \begin{bmatrix} i_L \\ j_L \\ k_L \end{bmatrix} \qquad [C.1]$$

The relative velocity vector is defined as:

$$V_C = [V_X \; V_Y \; V_Z] \begin{bmatrix} i \\ j \\ k \end{bmatrix} \qquad [C.2]$$

Using eq. C.1, eq. C.2 becomes

$$V_C = \begin{bmatrix} V_X\cos\sigma_A\cos\sigma_E + V_Y\sin\sigma_A\cos\sigma_E + V_Z\sin\sigma_E \\ -V_X\sin\sigma_A + V_Y\cos\sigma_A \\ -V_X\cos\sigma_A\sin\sigma_E - V_Y\sin\sigma_E\sin\sigma_A + V_Z\cos\sigma_E \end{bmatrix} \begin{bmatrix} i_L \\ j_L \\ k_L \end{bmatrix} \qquad [C.3]$$

The range vector coincides with the X axis. Then,

$$V_C = \dot{R} = \dot{R}i_L + R\dot{i}_L$$

$$= \dot{R}i_L + R\dot{\sigma}_A(-\cos\sigma_E\sin\sigma_A i + \cos\sigma_E\cos\sigma_A j) +$$

$$R\dot{\sigma}_E(-\cos\sigma_A\sin\sigma_E i - \sin\sigma_A\sin\sigma_E j + \cos\sigma_E K) \qquad [C.4]$$

Taking the inverse of eq. C.1 and substituting into eq. C.4 give:

$$V_C = \dot{R}i_L + R\dot{\sigma}_A\cos\sigma_E j_L + R\dot{\sigma}_E k_L \qquad [C.5]$$

Finally, equating components in eq. C.3 and eq. C.5 yields the range rate and the line-of-sight rate equations (eqs. 30 to 32).

The distance of closest approach of the missile to the target is illustrated in Fig. C1. It is assumed all missile and target accelerations are zero. From Fig. C1, the miss distance MD is given by:

$$MD = R\sin\beta = \frac{R|Ri_L|}{|V_C|} \qquad [C.6]$$

where β is the angle between the range vector and the closing velocity V_C.

Substituting eqs. C.4 and C.5 into C.6 gives:

$$MD = \frac{R^2(\dot{\sigma}_A^2\cos^2\sigma_E + R^2\dot{\sigma}_E^2)^{\frac{1}{2}}}{(\dot{R}^2 + R^2\cos^2\sigma_E\dot{\sigma}_A^2 + R^2\dot{\sigma}_E^2)^{\frac{1}{2}}} \qquad [C.7]$$

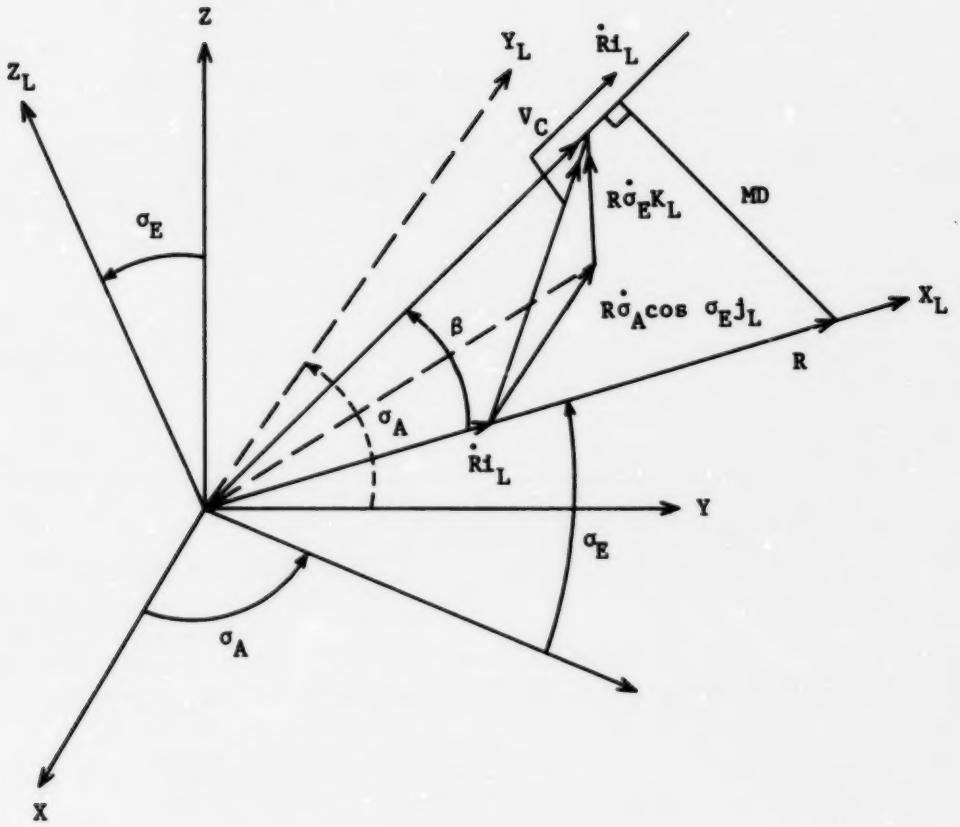

FIGURE C1 - Miss distance

APPENDIX D

Description and Operation of Digital Multiprocessor AD-10

The AD-10 is not a general-purpose computer capable of being programmed directly. As shown in Fig. D1, it requires the use of a host computer, the VAX 11/750, one of the VAX family of digital computers manufactured by Digital Equipment Corporation (DEC). The AD-10 software is designed to operate with the VAX/VMS operating system. The host computer is used to program the AD-10, to load the AD-10 program and memories, to debug the AD-10 program, to run the AD-10 diagnostics and to control in an interactive mode the AD-10 at run time. For these operations, the AD-10 appears as a peripheral device to the host computer. A graphic terminal connected to the VAX is used for the interactive control of the AD-10. The AD-10 solution can be observed on an X-Y display connected to the output of the D/A converters.

Figure D2 is a block diagram showing the architectural structure of the AD-10. The five processors of the AD-10 (Ref. D1), which are the COP (control processor), the MAP (memory address processor), the DEP (decision processor), the ARP (arithmetic processor) and the NIP (numerical integration processor), work in an overlapped and coordinated manner on different aspects of the simulation task. All processors, which communicate together through the multibus, synchronously execute instructions at a rate of 10 MHz. Each processor contains its own program counter and program memory. The ARP provides high-speed 16-bit arithmetic in 2's complement fractional and integer formats. Twenty additions and ten multiplications can be achieved each microsecond. The NIP uses a 48-bit word to represent the state variable in the AD-10. The COP coordinates the activities of the other fractional processors and provides the means to request service from the host computer. The MAP initiates data memory read and write operations and

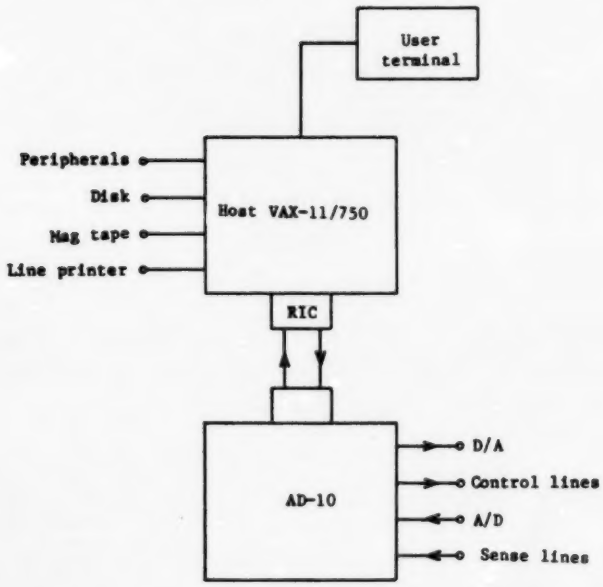

FIGURE D1 - AD-10 configuration

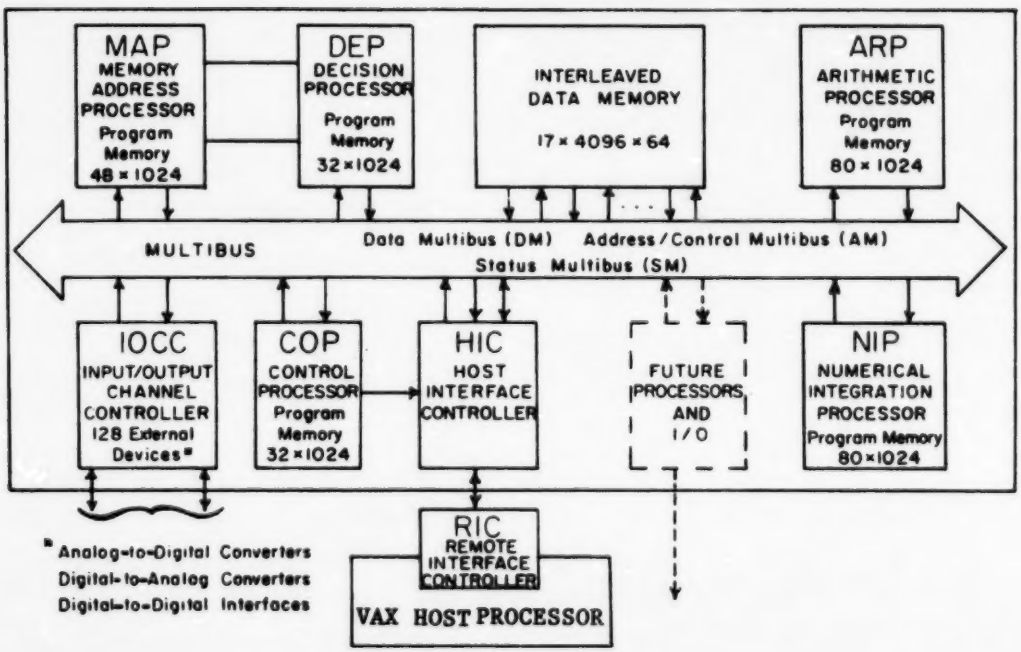

FIGURE D2 - AD-10 block diagram

may be viewed as the AD-10 data memory controller. Finally, the DEP executes comparison and modification instructions on a dual 128-word register file. This structure efficiently implements a binary search in function generation as well as other decision-oriented operations. The AD-10 has an input/output system that permits it to be interfaced directly to external devices. Analog-to-digital converters (ADCs), digital-to-analog converters (DACs), sense lines, control lines and a 16-bit parallel digital-to-digital interface are available as part of this I/O capability.

The advantages of the AD-10 parallelism and pipelining are made available through MPS-10, a modular programming method that translates the equations of the system to be simulated into machine language instructions and provides direct hands-on interaction at run time (Ref. D2). All the mathematical operations commonly used in dynamic simulation are grouped into program modules present in the AD-10. The programmer's task consists in linking these modules.

AD-10 codes are generated through MPS-10 and the host computer software. This software can be divided into four parts:

1. Create establishes the structure of the model by translating the source program into two files: one is a symbol table enabling operator interaction at run time. The other one is a data area file which establishes the sequence of equations' solution.

2. Specify orders indicates user default data: integration methods, frame time, speedup, output windowing, constant and parameter values. All this data can be changed at run time.

3. Relate links the default data to the simulation model, performs necessary mathematical operations on specific data and loads the results into the AD-10.

4. Interact provides all the data and simulation control information required for running the problem, loads the AD-10 program and data memory, allows the operator to change default values and relates them to the model while the problem is running.

With this approach to simulation modeling, the model is accessible at run time. Parameters, initial conditions and scale factors can all be changed. Integration algorithms can be specified. The display window and the variables to be displayed can be altered. Run-time solution control and time of solution can be modified. MPS-10 includes a range of mathematical modules linked directly to the AD-10 architecture. Each modular program derives argument and control direction through related data areas in the AD-10 data memory. The data areas are linked together to execute programs and can make use of the same modular program several times.

The MPS-10 library includes the following modules: the integrator summer linear and quadratic module accommodates a maximum of 48 inputs to form up to 24 outputs, either integrals of sums or simple sums. Currently, ten numerical integration methods are provided as subroutines in the NIP program memory. The algorithm to be used in integrating each state variable of the dynamic system mode must be specified. These methods are first-, second-, third- and fourth-order Adams-Bashforth predictors and Adams-Moulton predictor-correctors and the second- and fourth-order Runge-Kutta. The product modular program is used when a product of more than two variables is needed. The coordinate transformation modular program rotates coordinate systems through a maximum of six angles. The inverse resolution modular

program transforms up to three two-dimensional vectors from Cartesian to polar coordinates. The function interpolation program interpolates functions of up to four variables. The index and delta modular program supports the function interpolation modules by computing the pointers for many different function data tables. In addition to the mathematical modular program, modules for analog-to-digital and digital-to-analog conversion, digital-to-digital interface, comparator switch, logical program branching and control and sense-line support are also available.

REFERENCES

D1. "AD-10 Description", Applied Dynamic International, Ann Arbour, Michigan, 1981.

D2. "MPS 10 Reference Manual", Applied Dynamic International, Ann Arbour, Michigan, 1982.

DREV R-4389/86 (UNCLASSIFIED)

Research and Development Branch, DND, Canada.
DREV, P.O. Box 8800, Courcelette, Que. G0A 1R0

"Real-Time Simulation of Cruciform Short-Range Air-to-Air Guided Missiles"
by A. Morin

A six-degree-of-freedom missile simulation has been carried out in real time by a digital multiprocessor. The missile model and the simulation are described in this report. The simulation has also been verified by open- and closed-loop tests.

DREV R-4389/86 (UNCLASSIFIED)

Research and Development Branch, DND, Canada.
DREV, P.O. Box 8800, Courcelette, Que. G0A 1R0

"Real-Time Simulation of Cruciform Short-Range Air-to-Air Guided Missiles"
by A. Morin

A six-degree-of-freedom missile simulation has been carried out in real time by a digital multiprocessor. The missile model and the simulation are described in this report. The simulation has also been verified by open- and closed-loop tests.

DREV R-4389/86 (UNCLASSIFIED)

Research and Development Branch, DND, Canada.
DREV, P.O. Box 8800, Courcelette, Que. G0A 1R0

"Real-Time Simulation of Cruciform Short-Range Air-to-Air Guided Missiles"
by A. Morin

A six-degree-of-freedom missile simulation has been carried out in real time by a digital multiprocessor. The missile model and the simulation are described in this report. The simulation has also been verified by open- and closed-loop tests.

DREV R-4389/86 (UNCLASSIFIED)

Research and Development Branch, DND, Canada.
DREV, P.O. Box 8800, Courcelette, Que. G0A 1R0

"Real-Time Simulation of Cruciform Short-Range Air-to-Air Guided Missiles"
by A. Morin

A six-degree-of-freedom missile simulation has been carried out in real time by a digital multiprocessor. The missile model and the simulation are described in this report. The simulation has also been verified by open- and closed-loop tests.

CRDV R-4389/86 (SANS CLASSIFICATION)

Bureau - Recherche et Développement, MDN, Canada.
CRDV, C.P. 8800, Courcelette, Qué. G0A 1R0

"Simulation en temps réel de missiles guidés air-air, cruciformes et à courte portée"
par A. Morin

La simulation d'un missile comportant six degrés de liberté a été réalisée en temps réel à l'aide d'un multiprocesseur numérique. Le modèle du missile et la simulation sont décrits dans ce rapport. La simulation a aussi été vérifiée par des essais en boucle ouverte et fermée.

CRDV R-4389/86 (SANS CLASSIFICATION)

Bureau - Recherche et Développement, MDN, Canada.
CRDV, C.P. 8800, Courcelette, Qué. G0A 1R0

"Simulation en temps réel de missiles guidés air-air, cruciformes et à courte portée"
par A. Morin

La simulation d'un missile comportant six degrés de liberté a été réalisée en temps réel à l'aide d'un multiprocesseur numérique. Le modèle du missile et la simulation sont décrits dans ce rapport. La simulation a aussi été vérifiée par des essais en boucle ouverte et fermée.

CRDV R-4389/86 (SANS CLASSIFICATION)

Bureau - Recherche et Développement, MDN, Canada.
CRDV, C.P. 8800, Courcelette, Qué. G0A 1R0

"Simulation en temps réel de missiles guidés air-air, cruciformes et à courte portée"
par A. Morin

La simulation d'un missile comportant six degrés de liberté a été réalisée en temps réel à l'aide d'un multiprocesseur numérique. Le modèle du missile et la simulation sont décrits dans ce rapport. La simulation a aussi été vérifiée par des essais en boucle ouverte et fermée.

CRDV R-4389/86 (SANS CLASSIFICATION)

Bureau - Recherche et Développement, MDN, Canada.
CRDV, C.P. 8800, Courcelette, Qué. G0A 1R0

"Simulation en temps réel de missiles guidés air-air, cruciformes et à courte portée"
par A. Morin

La simulation d'un missile comportant six degrés de liberté a été réalisée en temps réel à l'aide d'un multiprocesseur numérique. Le modèle du missile et la simulation sont décrits dans ce rapport. La simulation a aussi été vérifiée par des essais en boucle ouverte et fermée.